AD-A041 135 FRANK J SEILER RESEARCH LAB UNITED STATES AIR FORCE --ETC F/G 20/6
ADAPTIVE ESTIMATION OF ABERRATION COEFFICIENTS IN ADAPTIVE OPTI--ETC(U)
MAY 77 R B ASHER, R D NEAL

UNCLASSIFIED FJSRL-TR-77-0009 NL

1 OF 1
ADA
041135

END

DATE
FILMED
7-77

(12)

FRANK J. SEILER RESEARCH LABORATORY

SRL-TR-77-0009

MAY 1977

ADAPTIVE ESTIMATION OF ABERRATION COEFFICIENTS IN ADAPTIVE OPTICS

SCIENTIFIC REPORT

PROJECT 2304

AIR FORCE SYSTEMS COMMAND
UNITED STATES AIR FORCE

UNCLASSIFIED

SECURITY CLASSIFICATION OF THIS PAGE *(When Data Entered)*

REPORT DOCUMENTATION PAGE

READ INSTRUCTIONS BEFORE COMPLETING FORM

1. REPORT NUMBER: FJSRL-TR-77-0009 AD-A
2. GOVT ACCESSION NO.
3. RECIPIENT'S CATALOG NUMBER

4. TITLE (and Subtitle): ADAPTIVE ESTIMATION OF ABERRATION COEFFICIENTS IN ADAPTIVE OPTICS
5. TYPE OF REPORT & PERIOD COVERED: Scientific
6. PERFORMING ORG. REPORT NUMBER

7. AUTHOR(s): Robert B. Asher, Robert D. Neal
8. CONTRACT OR GRANT NUMBER(s)

9. PERFORMING ORGANIZATION NAME AND ADDRESS: Frank J. Seiler Research Laboratory (AFSC), USAF Academy, Colorado 80840
10. PROGRAM ELEMENT, PROJECT, TASK AREA & WORK UNIT NUMBERS: DRS 61102F, 2304-F1-56

11. CONTROLLING OFFICE NAME AND ADDRESS: Frank J. Seiler Research Laboratory (AFSC), USAF Academy, Colorado 80840
12. REPORT DATE: May 1977
13. NUMBER OF PAGES: 31

14. MONITORING AGENCY NAME & ADDRESS *(if different from Controlling Office)*: 34p.
15. SECURITY CLASS. *(of this report)*: UNCLASSIFIED
15a. DECLASSIFICATION/DOWNGRADING SCHEDULE

16. DISTRIBUTION STATEMENT *(of this Report)*

Approved for public release; distribution unlimited.

17. DISTRIBUTION STATEMENT *(of the abstract entered in Block 20, if different from Report)*

18. SUPPLEMENTARY NOTES

19. KEY WORDS *(Continue on reverse side if necessary and identify by block number)*

Adaptive Optics
Adaptive Estimation

20. ABSTRACT *(Continue on reverse side if necessary and identify by block number)*

There are significant optical wavefront perturbational effects in the use of lasers and in imaging through atmospheric turbulence. In adaptive optics, an active element such as a deformable mirror is used to eliminate the phase aberrations of an optical wavefront. Diagnostics to determine the phase distortions are obtained by various methods. The deformable mirror is used in a feedback loop in order to cancel the unwanted phase distortions.

next page

DD FORM 1 JAN 73 1473 EDITION OF 1 NOV 65 IS OBSOLETE

UNCLASSIFIED

SECURITY CLASSIFICATION OF THIS PAGE *(When Data Entered)*

319920

Abstract (cont)

cont

This paper considers what is known as a modal approach to the adaptive optics problem in which the wavefront distortions are expanded into a spatial set of polynomials. The coefficients of the polynomials are temporally varying and represent the time varying phenomenological perturbations such as atmospheric turbulence, thermal blooming, and mirror distortions. The measurement devices for the wavefront are either a shearing interferometer or a Hartmann array. The shearing interferometer displaces or shears the wavefront and then interferes the sheared image with the unsheared image. The Hartmann array yields a linear measurement of the aberration coefficients through an effective measurement of the gradient of the wavefront. Since the wavefront is temporally varying, state space models for the aberration coefficients are obtained. An adaptive estimator is developed in order to adapt upon the atmospheric turbulence structure constant and the bandwidth of the atmospheric turbulence, and to then obtain a minimum mean square estimator for the aberration coefficients.

ADAPTIVE ESTIMATION OF ABERRATION COEFFICIENTS IN ADAPTIVE OPTICS

by

[+]Robert B. Asher
F.J. Seiler Research Laboratory
U.S. Air Force Academy, Colorado

and

[++]Robert D. Neal
Air Force Weapons Laboratory
Kirtland AFB, New Mexico

[+] Research Associate

[++]Chief, Short Range Applied Technology

Abstract

There are significant optical wavefront perturbational effects in the use of lasers and in imaging through atmospheric turbulence. In adaptive optics, an active element such as a deformable mirror is used to eliminate the phase aberrations of an optical wavefront. Diagnostics to determine the phase distortions are obtained by various methods. The deformable mirror is used in a feedback loop in order to cancel the unwanted phase distortions.

This paper considers what is known as a modal approach to the adaptive optics problem in which the wavefront distortions are expanded into a spatial set of polynomials. The coefficients of the polynomials are temporally varying and represent the time varying phenomenological perturbations such as atmospheric turbulence, thermal blooming, and mirror distortions. The measurement devices for the wavefront are either a shearing interferometer or a Hartmann array. The shearing interferometer displaces or shears the wavefront and then interferes the sheared image with the unsheared image. The Hartmann array yields a linear measurement of the aberration coefficients through an effective measurement of the gradient of the wavefront. Since the wavefront is temporally varying, state space models for the aberration coefficients are obtained. An adaptive estimator is developed in order to adapt upon the atmospheric turbulence structure constant and the bandwidth of the atmospheric turbulence, and to then obtain a minimum mean square estimator for the aberration coefficients.

I. Introduction

In order to obtain the maximum irradiance of a laser beam on a distant object, it is necessary to precisely control the position of the beam on the object. The pointing control is a precision closed loop feedback system which uses feedback measurements relative to where the beam is currently pointing in order to correct for deviations from where it should be pointed. This is certainly an important element in order to obtain maximum irradiance over a period of time. However, without further consideration the beam propagation to the object is in essence an open loop element in such a system. That is, there is no feedback as to the quality of the beam as it reaches the object. Thus, the beam is free to propagate according to the

current physical conditions. Since the propagation is affected by certain physical phenomenon, the beam quality at the object will be reduced yielding a reduction in the irradiance. These physical perturbational effects include the initial laser wavefront phase error, aberrations in the optical train, atmospheric turbulence, and atmospheric thermal blooming. These perturbational effects cause amplitude losses and phase distortions. The phase changes across the spatial extent of the beam causes destructive interference at the range of the object. The irradiance losses due to the phase distortions can be quite severe. Consequently, it is desirable to obtain feedback information as to the beam quality at the object such that the beam wavefront exiting at the aperture can be phase controlled. The phase control is introduced such that at the object range the beam will constructively interfere to create maximum irradiance. In this way, the beam is no longer an open loop element in the system but becomes a closed loop subsystem yielding all the desirable features of closed loop control such as error correction and insensitivity.

The technology area of phase control of modification of the wavefront exiting the aperture is known as adaptive optics. Basically, this technology requires a wavefront diagnostic subsystem in order to determine the beam quality at the object. The beam quality is diagnosed in order to obtain a measure of the deviation of the wavefront from a desired condition. The controller subsystem uses the wavefront diagnostics to calculate the required movement of the controlled element in order to obtain the necessary phase modifications. The controlled element can be a continuous, deformable mirror or segmented mirrors that are positioned in order to create the necessary phase changes in the outgoing wavefront. The objective, again, is to create the necessary phase changes in order to obtain constructive interference at the object range for maximum intensity.

The use of the philosophy of adaptive optics is not limited to laser applications. It can be used to correct imaging system optics. This correction is to compensate for deviations in the object wavefront due to perturbational effects such as atmospheric turbulence. Thereby high quality imaging may be accomplished.

There has been considerable effort in the use of this technology for both laser and imaging applications. In references [1,2,3] a segmented

mirror dither approach is considered. In particular, the beam is split into several segments which are mdoulated at different frequencies by dither mirrors. A detector measures the reflected intensity level modulated at the different dither frequencies. Synchronous detectors were used to detect and obtain a correction signal to be added to the mirror tilt such that the field phasors become nearly aligned at the object. This condition will yield maximum irradiance. Reference [4] considers the use of estimation and control in multidither adaptive optics. In reference [5] a cassegrain telescope is autofocused by use of a sinusoidal perturbation type adaptive control system. The focal plane for the converging beam is adjusted in order to coincide with the object range. This yields [6], the maximum beam irradiance on the object. Reference [13] is devoted to the optical technology of adaptive optics. This issue contains numerous papers on phase conjugate transmitter systems, image sharpening systems, transmitter multidither systems, and compensated imaging. Another approach to adaptive optics is the utilization of Bragg diffraction [14,15,16] in order to obtain a change in the index of refraction by modulating air with a sound wave.

There has been considerable interest and effort in using a closed loop concept in optical systems for astronomical telescopes [7-12]. In this application the telescope mirror surfaces are disturbed due to structural and thermal deformations. A figure sensor is used to obtain the actual, distorted, mirror figure. This measurement is compared against the desired figure and control actuators and commanded to position the mirror surface to minimize the error. In reference [11], a measure of image sharpness is used as a performance index from which a self-optimizing control system is used to phase control the incoming wavefront to eliminate phase distortions. See reference [13] for other papers on image sharpening.

The first step in obtaining maximum irradiance on an object or for image compensation is that of wavefront diagnostics. This yields a measure of the wavefront distortion in order to find the correction signal to the control elements. The control elements can be the adjustment of the focal length of a Cassegrain telescope by changing the distance between the primary and secondary mirrors [4,5], the control of a tilt mirror, and/or the control of a deformable mirror.

The measurements of the wavefront distortions are noisy. In particular, detector noise, background noise, and photon noise for photon limited applications limit the accuracy of measurement of the distortions. This paper develops the optimal estimator for estimating the wavefront distortions with two types of measurement devices, a shearing interferometer and a Hartmann array. Although these are two physically different optical devices, the mathematics of the measurements are similar. The estimators are, thus, similar and it is reasonable to consider both in the same paper.

The distortions are expanded into an orthonormal set of polynomials where the coefficients are called aberration coefficients. This corresponds to the proper optics terminology and the coefficients correspond to well known optical errors such as focus, astigmatism, coma, etc. The aberration coefficient temporal properties are modeled as linear Markov models. The bandwidths of the models are directly proportional to the relative wind speed across the optical aperture. The driving noise variance is directly proportional to the atmospheric turbulence structure constant, C_n^2 (see reference [17]).

This paper is the first application of adaptive estimation to adaptive optics. The adaptive estimator converges readily to the required estimates of the aberration coefficients in the presence of uncertain atmospheric turbulence. Thus, the adaptive estimation of aberration coefficients in adaptive optics is an extremely useful and important technique to enhance performance of high energy lasers and to enhance performance of imaging systems. The adaptive optics application represents a state of the art area in optics. Thus, the paper contributes also to the optical literature.

The paper is broken into six sections. Section II contains the problem statement. Section III gives the measurement devices and their equations. Section IV considers the dynamic models for the aberrations. Section V contains the formulation of the adaptive estimator, and Section VI contains the application of the estimator to the shearing interferometer problem.

II. Problem Statement

In order to correct the wavefront of an optical beam, it is necessary to spatially modify the phase of the beam. There are several ways of accomplishing a phase change, i.e., phase plates [18], Bragg diffraction,

focal length and tilt adjustment, and/or deformable mirrors. There is a need to change the phase in real-time in order to compensate for temporally as well as spatially changing distortions, and do this with low power requirements. In high energy laser applications, the most viable methods are that of focal length and tilt adjustment with higher order aberration correction using a deformable mirror. The mirrored surfaces must be cooled, however.

The intensity of a laser beam at the far field is a mapping of the phase as well as the amplitude [18,19]. A ratio of the ideal intensity without phase distortions, I^*, to the intensity with phase distortions, I, is called the Strehl ratio, i.e.,

$$i = \frac{I}{I^*} . \tag{1}$$

It may be shown [18] that the Strehl ratio is always less than one in the presence of phase distortions. High quality imagery also requires that the phase distortions be zero. The effect is shown symbolically in Figure 1.

In both the problems of imaging and high energy lasers, atmospheric turbulence acts to phase distort the optics. In addition, base vibrations cause effective phase distortions, thermal blooming of high energy lasers are a problem, and even the resonance in the laser cavity cause distortion problems. However, if the phase distortions, $\phi(x,y)$, were known over all the spatial regime, then a deformable mirror along with focus and tilt adjustment can be used to eliminate much of the distortion. In order to accomplish this diagnostic problem, the wavefront distortions, $I(x,y)$ may be expanded into a set of spatial polynomials defined over the spatial extent of the aperture. In particular, the polynomials are chosen to be orthogonal over the aperture. Two sets are common in optics work. The first set of polynomial expansions is known as Zernike polynomials [18]. The second set is used originally by Fried [17] and later by Hogge [20] in atmospheric turbulence work. The second expansion can be defined as follows

$$\phi(x,y) = \sum_{j=1}^{\infty} a_j F_j(x,y) \tag{2}$$

where the domain of definition for x and y is the circular region of the aperture. The a_j's are the aberration coefficients and F_j are a set of orthonormal polynomials related to the Zernike polynomial. The first ten polynomials and their physical significance are given below.

$$F_1(x,y) = \left(\frac{1}{\pi R^2}\right)^{\frac{1}{2}}, \qquad \text{(uniform phase shift across the aperture)}$$

$$\left.\begin{aligned} F_2(x,y) &= \left(\frac{4}{\pi R^4}\right)^{\frac{1}{2}} x, \\ F_3(x,y) &= \left(\frac{4}{\pi R^4}\right)^{\frac{1}{2}} y, \end{aligned}\right\} \quad \text{(tilt across aperture)}$$

$$F_4(x,y) = \left(\frac{12}{\pi R^6}\right)^{\frac{1}{2}} \left(x^2 + y^2 - \frac{R^2}{2}\right), \qquad \text{(refocus)}$$

$$\left.\begin{aligned} F_5(x,y) &= \left(\frac{6}{\pi R^5}\right)^{\frac{1}{2}} (x^2 - y^2), \\ F_6(x,y) &= \left(\frac{24}{\pi R^6}\right)^{\frac{1}{2}} (x \cdot y), \end{aligned}\right\} \quad \text{(astigmatism)} \qquad (3)$$

$$\left.\begin{aligned} F_7(x,y) &= \left(\frac{8}{\pi R^8}\right)^{\frac{1}{2}} (y^3 - 3xy^2), \\ F_8(x,y) &= \left(\frac{8}{\pi R^8}\right)^{\frac{1}{2}} (y^3 - 3yx^2), \\ F_9(x,y) &= \left(\frac{8}{\pi R^8}\right)^{\frac{1}{2}} (3x^2 + 3y^2 - 2R^2)x, \\ F_{10}(x,y) &= \left(\frac{8}{\pi R^8}\right)^{\frac{1}{2}} (3x^2 + 3y^2 - 2R^2)y \end{aligned}\right\} \quad \text{(coma)}$$

where R is the radius of the aperture. Fried [17] shows that when the wavefront is distorted by atmospheric turbulence, the lower order aberrations are the dominant terms. Furthermore, due to the fact that other physical phenomenon such as thermal blooming and mirror thermal distortions are also adequately represented by the low order aberrations, the wavefront distortions may be adequately assumed to be represented as a finite polynomial

$$\phi(x,y) = \sum_{j=1}^{\infty} a_j F_j(x,y). \tag{4}$$

In atmospheric turbulence, the aberration coefficients are not constant. Rather, they are temporally varying with bandwidth related to the relative wind speed across the aperture and with variance that is a function of the turbulence structure constant, C_n^2, which is a measure of the turbulence strength. Thus, it is more appropriate to write equation (4) as

$$\phi(x,y,t) = \sum_{j=1}^{n} a_j(t) F_j(x,y). \tag{5}$$

Given the phase distortions as in equation (5), the deformable mirror may be controlled to have a phase equal and opposite the phase distortions such that the total phase is zero. This leads to another reason, less physical than the dominance of the lower order terms, for the expansion of ϕ into a finite polynomial. That is, the control of the deformable mirror is limited to the highest spatial frequencies (as well as temporal bandwidth) that may be controlled due to the finite spacing of control actuators on the mirror.

In atmospheric turbulence, the image of the far field may be used to determine the phase distortions from which the reciprocity principle may be used to then cancel the phase via the deformable mirror control. Systems which use this type of wavefront measurement are known as image compensating systems [13]. A measurement of the phase distortions from the image may be obtained by using a shearing interferometer or by a Hartmann array. The measurements of these devices may be related to the aberration coefficients plus noise. The dynamic model for the aberrations are uncertain models in that they depend upon knowledge of the relative wind speed as well as the turbulence structure constant. Since the measurements are noisy and the

dynamic models contain uncertain parameters, it is necessary to use adaptive estimation in order to obtain an estimator for the coefficients. An important aspect of applications of the estimator is that the convergence times required are extremely fast. Thus, the adaptive estimation scheme chosen includes a probability estimator for the uncertain coefficients although the computational burden is greater than other adaptive estimation schemes, the convergence times required justify the use of this algorithm. The next section gives a basic description of the measurement devices as well as their equations.

III. Measurement Devices

There are two major measurement devices used in image compensation systems. The first is that of a shearing interferometer and the second is that of a Hartmann array. The measurement of the wavefront using a shearing interferometer is depicted in Figure 2 for a one directional shear. The wavefront is sheared in two orthogonal directions. The interference wavefront in one direction may be written as

$$V(x,y;s_x,t) = \phi(x+s_x,y,t) - \phi(x,y,t) \tag{6}$$

where ϕ is the phase front under test, s_x is the lateral shear direction, and V is the quantity to be measured.

Detector arrays behind the wavefront interferometer using zero crossing will measure the wavefront plus noise. Thus (assuming that two detector arrays are available to measure the vertical and the horizontal shear), the measurements for the i-th detector in each array is given as

$$V_{i,j}(x,y;s_j,t) = \phi_{ij}(x+s_j\delta_{xj},y+s_j\delta_{yj},t) - \phi(x_{iy},t) + \eta_{ij}, \tag{7}$$

$$i = 1,2,\ldots,q$$

$$j = x,y$$

where δ_{xj} and δ_{yj} are zero when $x \neq j$ or $y \neq j$ respectively, and when i represents the i-th detector in the j-th array (q detectors in each array), j = x corresponds to a horizontal shear, j = y corresponds to a vertical shear, and η_{ij} is the detector noise on the i-j-th detector. The noise η_{ij}

is assumed to be zero mean, white with covariance r_{ij}. It is assumed that the detector noise terms are independent of other detectors. The shearing distance is chosen equal to the separation of the detectors in the array. The wavefront measurements may be placed into an array

$$y = T\Phi + n \tag{8}$$

where y is a vector

$$y^T = \left[v_{1,x}, v_{2,x}, \ldots, v_{q,x}, v_{1,y}, v_{2,y}, \ldots, v_{q,y}\right]^T,$$

Φ is a vector formed from the independent phases in equation (7), and n is a noise vector, zero mean, white with diagonal covariance

$$E\left\{n(t)n(\tau)^T\right\} = R\delta(t-\tau)$$

where R is diagonal with elements r_{ii}. The measurements in equation (7) will be such that some of the Φ_{ij} and Φ_i will correspond to the same spatial phases. Thus, there will only be a fewer number of phases than 4q phases. Th matrix T is a matrix of plus and minus ones and zeros. A typical example is shown in Figure 3 in which the shear measurements may be written in terms of the phase values at the i-th spatial position. The 12 measurements in vector form are

$$\begin{bmatrix} y_1 \\ y_2 \\ y_3 \\ y_4 \\ y_5 \\ y_6 \\ y_7 \\ y_8 \\ y_9 \\ y_{10} \\ y_{11} \\ y_{12} \end{bmatrix} = \begin{bmatrix} -1 & 1 & 0 & 0 & 0 & 0 & 0 & 0 & 0 \\ 0 & -1 & 1 & 0 & 0 & 0 & 0 & 0 & 0 \\ 0 & 0 & 0 & -1 & 1 & 0 & 0 & 0 & 0 \\ 0 & 0 & 0 & 0 & -1 & 1 & 0 & 0 & 0 \\ 0 & 0 & 0 & 0 & 0 & 0 & -1 & 1 & 0 \\ 0 & 0 & 0 & 0 & 0 & 0 & 0 & -1 & 1 \\ 1 & 0 & 0 & -1 & 0 & 0 & 0 & 0 & 0 \\ 0 & 1 & 0 & 0 & -1 & 0 & 0 & 0 & 0 \\ 0 & 0 & 1 & 0 & 0 & -1 & 0 & 0 & 0 \\ 0 & 0 & 0 & 1 & 0 & 0 & -1 & 0 & 0 \\ 0 & 0 & 0 & 0 & 1 & 0 & 0 & -1 & 0 \\ 0 & 0 & 0 & 0 & 0 & 1 & 0 & 0 & -1 \end{bmatrix} \begin{bmatrix} \Phi_1 \\ \Phi_2 \\ \Phi_3 \\ \Phi_4 \\ \Phi_5 \\ \Phi_6 \\ \Phi_7 \\ \Phi_8 \\ \Phi_9 \end{bmatrix} + \begin{bmatrix} \eta_{x_1} \\ \eta_{x_2} \\ \eta_{x_3} \\ \eta_{x_4} \\ \eta_{x_5} \\ \eta_{x_6} \\ \eta_{y_1} \\ \eta_{y_2} \\ \eta_{y_3} \\ \eta_{y_4} \\ \eta_{y_5} \\ \eta_{y_6} \end{bmatrix} \tag{9}$$

The wavefront distortions may be expanded into the polynomials as in equation (5), i.e.,

$$\Phi(x_i,y_i,t) = \sum_{j=1}^{n} a_j(t) F_j(x_i,y_i) \tag{10}$$

where (x_i,y_i) corresponds to the i-th spatial point. Thus, a vector equation may be written for the phases in terms of the aberration coefficients, i.e.,

$$\begin{bmatrix} \Phi_1 \\ \Phi_2 \\ \Phi_3 \\ \cdot \\ \cdot \\ \cdot \\ \Phi_m \end{bmatrix} = \begin{bmatrix} F_1(x_1,y_1), & F_2(x_1,y_1), & \ldots, & F_n(x_1,y_1) \\ F_1(x_2,y_2), & F_2(x_2,y_2), & \ldots, & F_n(x_2,y_2) \\ F_1(x_3,y_3), & F_2(x_3,y_3), & \ldots, & F_n(x_3,y_3) \\ \cdot & \cdot & & \cdot \\ \cdot & \cdot & & \cdot \\ \cdot & \cdot & & \cdot \\ F_1(x_m,y_m), & F_2(x_m,y_m), & \ldots, & F_n(x_m,y_m) \end{bmatrix} \begin{bmatrix} a_1(t) \\ a_2(t) \\ a_3(t) \\ \cdot \\ \cdot \\ \cdot \\ a_m(t) \end{bmatrix} \tag{11}$$

or equation (11) may be written in vector form as

$$\Phi = Fa(t). \tag{12}$$

Equation (12) may be used with equation (8) to obtain a measurement equation in terms of the aberration coefficients, i.e.,

$$\begin{aligned} y &= (TF)a + \eta \\ &= H_{SI}a + \eta \end{aligned} \tag{13}$$

where the definition of H_{SI} is obvious and the subscript, SI, denotes the measurements using a shearing interferometer. This is the desired measurement equation for the shearing interferometer.

The measurement of the wavefront using a Hartmann array is depicted in Figure 4. Basically, the image is formed on the Hartmann array by a lens system. Since the distance to the object is long, a wavefront impinging on the array would be approximately planar without turbulence effects. However, turbulence distorts the phase of the wavefront as in Figure 1. Thus, the image across the Hartmann array is phase distorted in the presence of atmospheric turbulence. The Hartmann array consists of several hundred pinholes (or fly eye lenses) that deflect the light back to quad detectors located behind each hole (or lens). The quad detectors will yield measurements proportional to the gradient of the wavefront in both x and y directions, i.e., for each pinhole two measurements are obtained, i.e.,

$$\theta_{x_i} = \frac{\partial \Phi_i}{\partial x} + \eta_{x_i}, \quad i=1,2,\ldots,q \tag{14}$$

and

$$\theta_{y_i} = \frac{\partial \Phi_i}{\partial y} + \eta_{y_i}, \quad i=1,2,\ldots,q \tag{15}$$

where q is the number of pinhole-detector pairs. The gradient of the wavefront in terms of the aberration coefficients may be obtained by differentiating equation (5), i.e.,

$$\frac{\partial \Phi(x_i,y_i)}{\partial x} = \sum_{j=1}^{n} a_j(t) \frac{\partial F_j(x_i,y_i)}{\partial x}, \tag{16}$$

$$i=1,2,\ldots,q,$$

and

$$\frac{\partial \Phi(x_i, y_i)}{\partial y} = \sum_{j=1}^{n} a_j(t) \frac{\partial F_j(x_i, y_i)}{\partial y} \tag{17}$$

Equations (14) and (15) may be put into vector form as

$$\begin{bmatrix} \theta_{v_1} \\ \theta_{y_1} \\ \theta_{x_2} \\ \theta_{y_2} \\ \vdots \\ \theta_{x_q} \\ \theta_{y_q} \end{bmatrix} = \begin{bmatrix} \frac{\partial F_1(x_1,y_1)}{\partial x}, & \frac{\partial F_2(x_1,y_1)}{\partial x}, & \ldots, & \frac{F_n(x_1,y_1)}{\partial x} \\ \frac{\partial F_1(x_1,y_1)}{\partial y}, & \frac{\partial F_2(x_1,y_1)}{\partial y}, & \ldots, & \frac{\partial F_n(x_1,y_1)}{\partial y} \\ \frac{\partial F_1(x_2,y_2)}{\partial x}, & \frac{\partial F_2(x_2,y_2)}{\partial x}, & \ldots, & \frac{\partial F_n(x_2,y_2)}{\partial x} \\ \frac{\partial F_1(x_2,y_2)}{\partial y}, & \frac{\partial F_2(x_2,y_2)}{\partial y}, & \ldots, & \frac{\partial F_n(x_2,y_2)}{\partial y} \\ \vdots \\ \frac{\partial F_1(x_q,y_q)}{\partial x}, & \frac{\partial F_2(x_q,y_q)}{\partial x}, & \ldots, & \frac{\partial F_n(x_q,y_q)}{\partial x} \\ \frac{\partial F_1(x_q,y_q)}{\partial y}, & \frac{\partial F_2(x_q,y_q)}{\partial y}, & \ldots, & \frac{\partial F_n(x_q,y_q)}{\partial y} \end{bmatrix} \begin{bmatrix} a_1(t) \\ a_2(t) \\ \vdots \\ a_n(t) \end{bmatrix} + \begin{bmatrix} \eta_{v_1} \\ \eta_{y_1} \\ \eta_{x_2} \\ \eta_{y_2} \\ \vdots \\ \eta_{x_q} \\ \eta_{y_q} \end{bmatrix} \tag{18}$$

or in vector form

$$y = H_{HA}\, a + \eta \tag{19}$$

where y is the measurement vector in equation (18), H_{HA} is the measurement matrix of partials, and η is the vector of measurement noises. The measurement noise is assumed zero-mean, white with covariance

$$E\{\eta(t)\eta(\tau)^T\} = R(t)\delta(t-\tau)$$

where R is in block diagonal form since the measurement noise η_{x_i} is correlated in general with η_{y_i}, $v_i = 1,2,\ldots,q$. This particular aspect

complicates the estimator somewhat as each pair of measurements for one detector must be processed through the estimator rather than sequentially processing each measurement. However, the form of the estimator is still simplified over the form required if R was not block diagonal.

This section then contains the development of the measurement equations for both the shearing interferometer and the Hartmann array image compensation systems. The equations are in the form of linear transformations of the aberration coefficients. This allows for the development of the instimation equations for both systems. The next section considers approximations for the state space models of the aberration coefficients.

IV. Dynamic Modeling of the Aberration Coefficients

In order to develop an estimator structure for the estimation of the aberration coefficients, it is necessary to obtain models for the temporal variation of the coefficients. The models must be such that they adequately represent the actual statistics of variation, and yet be simple enough for implementation into the filter. Furthermore, the models will be shown to be functions of the atmospheric turbulence bandwidth as well as the atmospheric turbulence structure constant, C_n^2 (see references [24, 25] for a precise definition). These models are approximations similar to that of reference [26] for the intensity fluctuations of a laser beam and similar to reference [27] for the temporal phase distortions. However, since the estimator is adaptive, it will adapt upon the best model structure for the particular realization of atmospheric turbulence. Also, the time interval for use of a high power laser as well as imaging through atmospheric turbulence is short. Thus, the models are adequate for this problem and will yield an estimator structure that can be implemented real time.

In Fried's paper [17] on wavefront distortion, it is shown that the mean square value of the linear tilt coefficients is given as

$$E(a_L^2) = 0.694D^2(D/r_o)^{5/3} \tag{20}$$

where a_L^2 is equal to $(a_2^2 + a_3^2)$, the mean square value of the spherical coefficients is given as

$$E(a_S^2) = 0.01657D^2(D/r_o)^{5/3}\,, \tag{21}$$

where a_4^2 is equal to a_5^2, and the mean square value of the quadratic coefficients is given as

$$E(a_Q^2) = 0.0527D^2(D/r_o)^{5/3} \tag{22}$$

where a_Q^2 is equal to $(a_4^2 + a_5^2 + a_6^2)$. The diameter of the aperture is denoted as D, and the quantity r_o is a length parameter defined as

$$r_o = (6.88/a)^{3/5} \tag{23}$$

where

$$a = 2.91(2\pi/\lambda)^2 \int_{path} C_n^2(s)Q(s)ds \tag{24}$$

where λ is the wavelength and where Q(D) is a weighting factor depending on the nature of the optical source. In the case of an infinite plane wave source with a constant structure constant, the parameter r_o is given as

$$r_o = \left[\frac{6.88}{2.91\ k^2 R C_n^2}\right]^{3/5} \text{ meters} \tag{25}$$

where $k = 2\pi/\lambda$ is the wavenumber, R is the range in meters, and C_n^2 is the turbulence structure constant which is a measure of turbulence strength. References [20, 28] discuss the temporal variation of the atmospheric turbulence. It is shown that the corner frequency of the turbulence for each aberration is of the order of the relative wind speed divided by the diameter of the aperture. In reference [28] approximations to the power spectral densities are given. It is assumed that adequate approximations to these models for each aberration are of the form

$$\dot{a}_i = -\beta_i a_i + \sqrt{2\beta_i}\ \sigma_i u_i, \tag{26}$$

$$i=2,3,\ldots,n,$$

where the β_i is given as

$$\beta_i = k_i \frac{V}{D} \tag{27}$$

with k_i given in Table I, where V is the relative wind velocity, and where a_i is zero mean white noise with unity variance. The variance σ_i may be calculated by use of Fried's paper. Thus, the terms are

$$\sigma_i = \sqrt{\frac{E(a_L^2)}{2}}, \quad i=2,3,$$
$$\sigma_4 = \sqrt{E(a_S^2)}, \tag{28}$$

and

$$\sigma_i = \sqrt{\frac{E(a_Q^2) - \sigma_4^2}{2}}, \quad i=5,6.$$

It is assumed in such a set of models that the aberrations are uncorrelated. They are not in the expansion functions as given in [20]. However, uncorrelated expansion functions may be found. Also, additional uncertain model parameters may be used to ascertain this correlation. These parameters may be augmented to the adaptive estimator.

The first coefficient which appears as a constant phase shift doesn't affect the far field intensity. It may be noted that the variances, σ_i, are functions of the turbulence structure constant. Since the turbulence strength is not known a priori for a ptach of turbulence, the structure constant, C_n^2, is uncertain. Furthermore, since the relative wind speed is not known precisely for an aircraft scenario, V may be uncertain. Thus, the estimator must adapt on the uncertain parameters in order to learn them for use in the estimation processes. Furthermore, structure adaptation may be used to refine the models for a particular realization if the time interval demands a more accurate model.

The model approximations are reasonable for the logic previously stated. That is, other work in laser fluctuations have used similar models, the estimator will adapt upon uncertain parameters, the analytics for turbulence may not correspond to a given scenario, and a computationally feasible model is necessary for real-time implementation.

The next section gives the structure of the adaptive estimator.

V. Adaptive Estimator

This section contains the equations for the adaptive estimator. The estimator is based upon the original work by Magill [29] and extended by Lainiotis [30] and Hawkes and Moore [31]. In particular, as the measurements for the shearing interferometer are in a form whereby the measurement noise covariance matrix is diagonal and as the measurements for the Hartmann array are in a form whereby the measurement noise covariance matrix is block diagonal with blocks of 2 x 2, the sequential processing adaptive estimation form of Hawkes and Moore is especially viable. In this form, the measurements may be processed in a sequential form (one at a time). This only requires a scalar inverse for the shearing interferometer measurement and a 2 x 2 inverse for the Hartmann array.

The dynamic equation for the aberration, equation (26), may be discretized as

$$a_i(k+1) = \exp(-\beta_i T) a_i(k) + q_i(k) u_i(k) \tag{29}$$

where

$$q_i(k) = \sqrt{\frac{E(a_i^2)}{2\beta_i}\left[1 - \exp(-2\beta_i T)\right]}$$

u_i is zero mean white noise with unity variance, and T is the sampling period. The dynamic equations may, thus, be written in the general form

$$a(k+1) = \Phi(v) a(k) + \Gamma(v, C_n^2) u(k) \tag{30}$$

where

$$\Phi(v) = \begin{bmatrix} \exp(-k_2 \frac{V}{D}) & 0 & 0 & 0 & 0 \\ 0 & \exp(-k_3 \frac{V}{D}) & 0 & 0 & 0 \\ 0 & 0 & \exp(-k_4 \frac{V}{D}) & 0 & 0 \\ 0 & 0 & 0 & \exp(-k_5 \frac{V}{D}) & 0 \\ 0 & 0 & 0 & 0 & \exp(-k_6 \frac{V}{D}) \end{bmatrix}$$

and where

$$\Gamma(v,C_n^2) = \begin{bmatrix} q_2(k) & 0 & 0 & 0 & 0 \\ 0 & q_3(k) & 0 & 0 & 0 \\ 0 & 0 & q_4(k) & 0 & 0 \\ 0 & 0 & 0 & q_5(k) & 0 \\ 0 & 0 & 0 & 0 & q_6(k) \end{bmatrix}$$

where

$$q_i(k) = q_i(k,v,C_n^2)$$

from the definition of $q_i(k)$. It is assumed that v and C_n^2 are defined over a discrete range. The two parameters may be contained in the finite set

$$v\varepsilon\{v_1,v_2,\ldots,v_{q_1}\}$$

and

$$C_n^2\varepsilon\{C_{n_1}^2,C_{n_2}^2,\ldots,C_{n_{q_2}}^2\}$$

with a priori probability density function

$$P(v) = \sum_{i=1}^{q_1} P_r(v_i)\delta(v-v_i)$$

and

$$P(C_n^2) = \sum_{i=1}^{q_2} P_r(C_{n_i}^2)\delta(C_n^2-C_{n_i}^2).$$

The a priori density function for the pair is given (assuming independence) as

$$P(v,C_n^2) = \sum_{i=1}^{q_1}\sum_{j=1}^{q_2} P_r(v_i)P_r(C_{n_j}^2)\delta(v-v_i,C_n^2-C_{n_j}^2) \qquad (31)$$

or by defining $\theta_i^T = \{v, C_n^2\}^T$

$$P(\theta) = \sum_{i=1}^{\bar{q}} P_r(\theta_i)\delta(\theta-\theta_{i_j}) \tag{32}$$

where θ_i is defined for each $q_1 \times q_2$ pair of v's and C_n^2's and $\bar{q} = q_1 \times q_2$.

The algorithm for the shearing interferometer measurements will be written explicitly for completeness. The Hartmann array algorithm is an immediate extension of this and will, thus, not be written.

Equation (13) may be partitioned as

$$H_{SI} = \begin{bmatrix} h_1 \\ h_2 \\ \vdots \\ h_{2q} \end{bmatrix} \tag{33}$$

where h_i is the i-th row of the matrix. The measurement equation may thus be written as

$$\begin{bmatrix} y_1 \\ y_2 \\ \vdots \\ y_{2q} \end{bmatrix} = \begin{bmatrix} h_1 a + n_1 \\ h_2 a + n_2 \\ \vdots \\ h_{2q} a + n_{2q} \end{bmatrix} \tag{34}$$

Using the results in [30], the optimal estimator for the aberration coefficients given the measurements up to and including time k is

$$\hat{a}^+(k|\psi_k) = \sum_{i=1}^{\bar{q}} \hat{a}^+(k|\psi_k,\theta_i)P_r(\theta_i|\psi_k). \tag{35}$$

where $\hat{a}^+(k|\psi_k,\theta_i)$ is the θ_i-conditional estimate for a and $P_r(\theta_i|\psi_k)$ is the probability of θ_i given the measurements. The covariance of this estimate is

$$P(k) = \sum_{i=1}^{\bar{q}} \left\{ P(k|\theta_i) + [\hat{a}(k|\psi_k,\theta_i) - \hat{a}^+(k|\psi_k)][\hat{a}^+(k|\psi_k,\theta_i) - \hat{a}^+(k|\psi_k)]^T \right\}. \quad (36)$$

The θ_i-conditional estimates may be found between measurements as

$$\hat{a}^-(k+1|\psi_k,\theta_i) = \Phi(\theta_i)\hat{a}^+(k|\psi_k,\theta_i), \quad (37)$$

$$i=1,2,\ldots,\bar{q}$$

and

$$P^-(k+1|\theta_i) = \Phi(\theta_i)P^+(k|\theta_i)\Phi^T(\theta_i) + \Gamma(\theta_i)\Gamma(\theta_i)^T, \quad (38)$$

$$i=1,2,\ldots,\bar{q}$$

where $\Phi(\theta_i)$ and $\Gamma(\theta_i)$ are as in equation (30) evaluated with the i-th θ. At a measurement the θ_i-conditional estimate may be found by sequentially processing the measurements through the following algorithm. The first measurement processing is

$$\hat{a}^{(1)}(k|\psi_{k-1},y_1,\theta_i) = \hat{a}^-(k|\psi_{k-1},\theta_i) + K_k^{(1)}(\theta_i)[y_1 - h_1 a^-(k|\psi_{k-1},\theta_i)], \quad (39)$$

$$i=1,2,\ldots,2q$$

where

$$K_k^{(1)}(\theta_i) = P^-(k|\theta_i)h_1^T[h_1 P^-(k|\theta_i)h_1^T + r_1]^{-1}, \quad (40)$$

$$i=1,2,\ldots,2q$$

where r_1 is the covariance of the final measurement noise element and $\hat{a}^{(1)}(k|\psi_{k-1},y_1,\theta_i)$ denotes the estimate given the past measurements and the measurement on the first row of the measurement vector. The covariance of this estimate is

$$P^{(1)}(k|\theta_i) = [I-K_k^{(1)}(\theta_i)h_1]P^-(k|\theta_i), \quad (41)$$

$$i=1,2,\ldots,2q$$

The required estimate is given by cycling through the iterations

$$\hat{a}^{(\ell)}(k|\psi_k,y_1,y_2,\ldots,y_\ell,\theta_i) = \hat{a}^{(\ell-1)}(k|\psi_k,y_1,y_2,\ldots,y_{\ell-1},\theta_i) +$$

$$K_k^{(\ell)}(\theta_i)[y_\ell - h_\ell \hat{a}^{(\ell-1)}(k|\psi_k,y_1,y_2,\ldots,y_{\ell-1},\theta_i)], \qquad (42)$$

$$\ell=2,3,\ldots,2q$$

where

$$K_k^{(\ell)}(\theta_i) = P^{(\ell-1)}(k|\theta_i)h_\ell^T[h_\ell P^{(\ell-1)}(k|\theta_i)\cdot h_\ell^T + r_\ell]^{-1} \qquad (43)$$

where r_ℓ is the covariance of the ℓ-th measurement noise element. The covariance update is given by

$$P^{(\ell)}(k|\theta_i) = [I-K_k^{(\ell)}(\theta_i)h_\ell]P^{(\ell-1)}(k|\theta_i), \qquad (44)$$

$$\ell=2,3,\ldots,2q$$

The required θ_i-conditional estimate is given by

$$\hat{a}^+(k|\psi_k,\theta_i) = \hat{a}^{(2q)}(k|\psi_k,\theta_i) \qquad (45)$$

and its covariance is given as

$$P^+(k|\theta_i) = P^{(2q)}(k|\theta_i). \qquad (46)$$

It may be noted that only a scalar inverse need be taken to find the required estimate. In order to update the necessary probabilities sequentially, it is necessary to store $[h_\ell P^{(\ell)}(k|\theta_i)h_\ell^T + r_\ell]$ and the residuals $y_\ell - h_\ell \hat{a}^{(\ell)}(k|\theta_i)$, for $\ell=1,2,\ldots,2q$ and $i=1,2,\ldots,\bar{q}$. These quantities are available as they are calculated from the previous equations. The required probabilities are then calculated as in reference [31], i.e.,

$$P_r(\theta_i|\psi_k) = \frac{\prod_{\ell=1}^{2q} |\psi_k^{(\ell)}(\theta_i)|^{-\frac{1}{2}} \exp\left\{-\frac{1}{2}[\nu_k^{(\ell)}(\theta_i)]^T[\Omega_k^{(\ell)}(\theta_i)]^{-1}[\nu_k^{(\ell)}(\theta_i)]\right\} P_r(\theta_i|\psi_{k-1})}{\sum_{i=1}^{q}\left\{\prod_{\ell=1}^{2q} |\psi_k^{(\ell)}(\theta_i)|^{-\frac{1}{2}} \exp\left\{-\frac{1}{2}[\nu_k^{(\ell)}(\theta_i)]^T[\Omega_k^{(\ell)}(\theta_i)][\nu_k^{(\ell)}(\theta_i)]\right\} P_r(\theta_i|\psi_{k-1})\right\}} \qquad (47)$$

for $i=1,2,\ldots,\bar{q}$ where

$$\nu_k^{(\ell)}(\theta_i) = y_\ell - h_\ell \hat{a}^{(\ell)}(k|\psi_{k-1}, y_1, y_2, \ldots, y_{\ell-1}, \theta_i) \tag{48}$$

and

$$\Omega_k^{(\ell)}(\theta_i) = [h_\ell P^{(\ell)}(k|\theta_j) h_\ell^T + r_\ell]. \tag{49}$$

The terms $\nu_k^{(\ell)}(\theta_i)$ and $\Omega_k^{(\ell)}(\theta_i)$ have been stored during the previous calculations.

VI. Results and Conclusions

The estimator was simulated for various types of lasers, several different propagation lengths, and several optical aperture diameters. The three types of lasers simulated were the gas dynamic laser (GDL) at 10.6×10^{-6} meter wavelength, the electric discharge laser (EDL) at 9.28×10^{-6} meter wavelength, and a chemical laser using deuterium floride (DF) at 3.69×10^{-6} meter wavelength. Both short ranges 1-5 kilometers and medium ranges 20-50 kilometers were used. Several different signal to noise ratios were used.

All units yield a phase error in radians. The tilt errors are, for example, in units of radians/meters. Since the resolution of any plots would be less than minimal because of the significant decrease in several orders of magnitude of the covariance of estimation error, plots of the results will not be shown. Instead, both the initial and steady state covariance of the estimation error for each case will be given for each aberration order. The steady state solution is a strong function of the measurement noise and less of a function of the dynamic models. The cases shown are for an approximate signal to noise ratio of five. The sample rate for the measurements is 0.0005 seconds. This is considered realistic with a state of the art computer. Five possible values of C_n^2 and the bandwidths were used. The actual C_n^2 for each run was 1×10^{-16}. The turbulence bandwidths were chosen with a transonic relative wind speed.

For the case of a GDL with one meter optics and a range of one kilometer, the initial standard deviation for the two tilts, refocus, and two astigmatisms were 0.7179, 1.56×10^{-1}, and 1.338×10^{-1}, respectively. In several

Monte Carlo runs, the correct parameters were learned before 0.02 seconds. The steady state standard deviation at 0.025 seconds after a measurement were as follows: x-tilt, 2.43×10^{-3}; y-tilt, 2.42×10^{-3}; refocus, 7.14×10^{-4}; quadratic astigmatism, 6.86×10^{-4}; and product astigmatism, 7.74×10^{-4}. The x-tilt, for example, would correspond to an uncertainty of 1.52×10^{-2} wavelengths. With an initial range of 50 kilometers, the initial standard deviations for the two tilts, refocus, and two astigmatisms were 5.259, 1.11, and 0.946, respectively. Again, the true parameters were learned before 0.02 seconds in several runs. The steady state standard deviations at 0.025 seconds after a measurement were as follows: x-tilt, 4.666×10^{-3}; y-tilt, 4.47×10^{-3}; refocus, 2.93×10^{-3}; quadratic astigmatism, 3.22×10^{-3}; and product astigmatism, 2.687×10^{-3}. It can be seen that the increase in propagation distance increases the initial and the final uncertainty. The tilt uncertainties at steady state are about doubled for an increase of range by 50 times.

For the case of a GDL with 0.6 meter optics and a range of 5 kilometers, the initial standard deviations for the two tilts, refocus, and two astigmatisms were 1.605, 3.51×10^{-1}, and 2.99×10^{-1}, respectively. In several Monte Carlo runs, the correct parameters were learned before 0.02 seconds. The steady state standard deviations at 0.025 seconds after a measurement were as follows: x-tilt, 3.46×10^{-3}; y-tilt, 3.38×10^{-3}; refocus, 1.415×10^{-3}; quadratic astigmatism, 1.419×10^{-3}; and product astigmatism, 1.413×10^{-3}.

For the case of an EDL with 0.6 meter optics and a range of 5 kilometers, the initial standard deviations for the two tilts, refocus, and two astigmatisms were 0.7187, 1.57×10^{-1}, and 1.339×10^{-1}, respectively. The correct parameters were learned before 0.035 seconds. The steady state standard deviations at 0.050 seconds after a measurement were as follows: x-tilt, 2.43×10^{-3}; y-tilt, 2.426×10^{-3}; refocus, 7.15×10^{-4}; quadratic astigmatism, 6.87×10^{-4}; and product astigmatism, 7.74×10^{-4}.

For the case of a DF laser with 0.6 meter optics and a range of 5 kilometers, the initial standard deviations for the two tilts, refocus, and two astigmatisms were 4.61, 1.008, and 8.59×10^{-1}, respectively. The steady state standard deviations at 0.02 seconds after a measurement were as

follows: x-tilt, 4.60 x 10^{-3}; y-tilt, 4.41 x 10^{-3}; refocus, 2.79 x 10^{-3}; quadratic astigmatism, 3.045 x 10^{-3}; and product astigmatism, 2.569 x 10^{-3}. With a range of 50 kilometers and 1 meter optics the initial standard deviations are respectively 14.58, 3.19, and 2.72. At steady state, the standard deviations are as follows: x-tilt, 5.11 x 10^{-3}; y-tilt, 4.85 x 10^{-3}; refocus, 4.39 x 10^{-3}; quadratic astigmatism, 5.338 x 10^{-3}; and product astigmatism, 3.93 x 10^{-3}.

It may be seen that, as is well known, the uncertainties for shorter wavelengths through atmospheric turbulence are initially greatly increased. However, the adaptive estimator is able to decrease this uncertainty, which is much higher than the uncertainties at larger wavelengths, to a value nearly the same as the larger wavelength lasers. The estimator is seen to bring the uncertainty levels down to that required for control while adapting upon the uncertain atmospheric turbulence strength and bandwidth. Other runs were accomplished at lower and higher signal to noise levels which indicate similar results.

This paper introduces the adaptive optics problem to the control community. The adaptive estimation structure developed within is a viable structure for estimation of aberration coefficients in adaptive optics systems. The estimator has been well exercised with several Monte Carlo runs for GDL, EDL, and DF lasers at several ranges and several different optical apertures. The estimator may be implemented into a minicomputer with either time varying or constant gains for real time applications.

Table 1
Coefficients for Bandwidth

j	k_j
2	0.53
3	0.33
4	1.1
5	0.9
6	0.6
7	0.8
8	1.4
9	1.3
10	1.1

UNCORRECTED LASER BEAM PROPAGATING THROUGH ATMOSPHERIC TURBULENCE

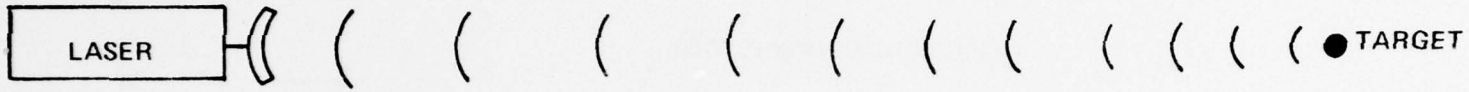

CORRECTED OR IDEAL BEAM

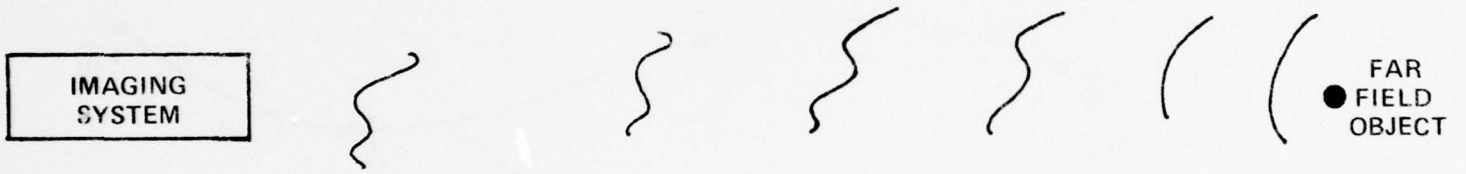

UNCORRECTED INAGE IN TURBULENCE

FIGURE 1 LASER AND IMAGE PROPAGATION THROUGH ATMOSPHERIC TURBULENCE

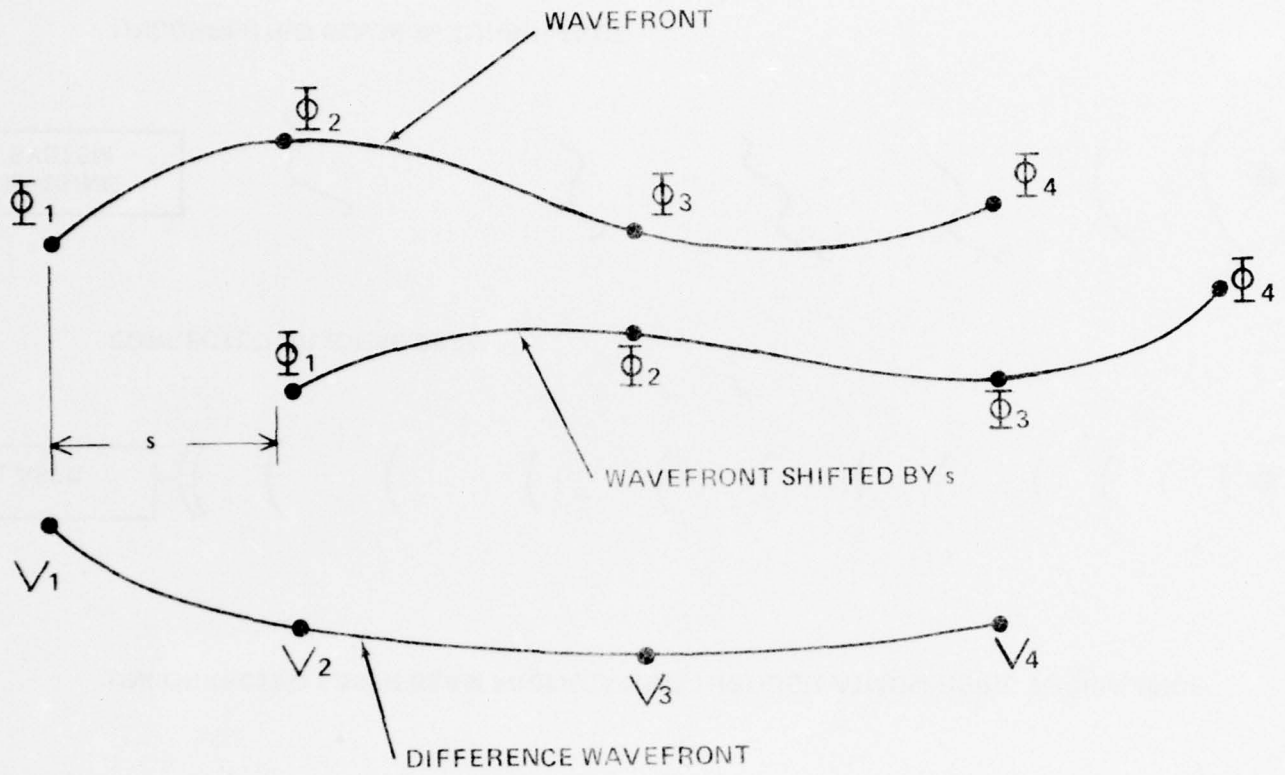

FIGURE 2 SCHEMATIC REPRESENTATION OF A ONE-DIMENSIONAL SHEARING INTERFEROMETER

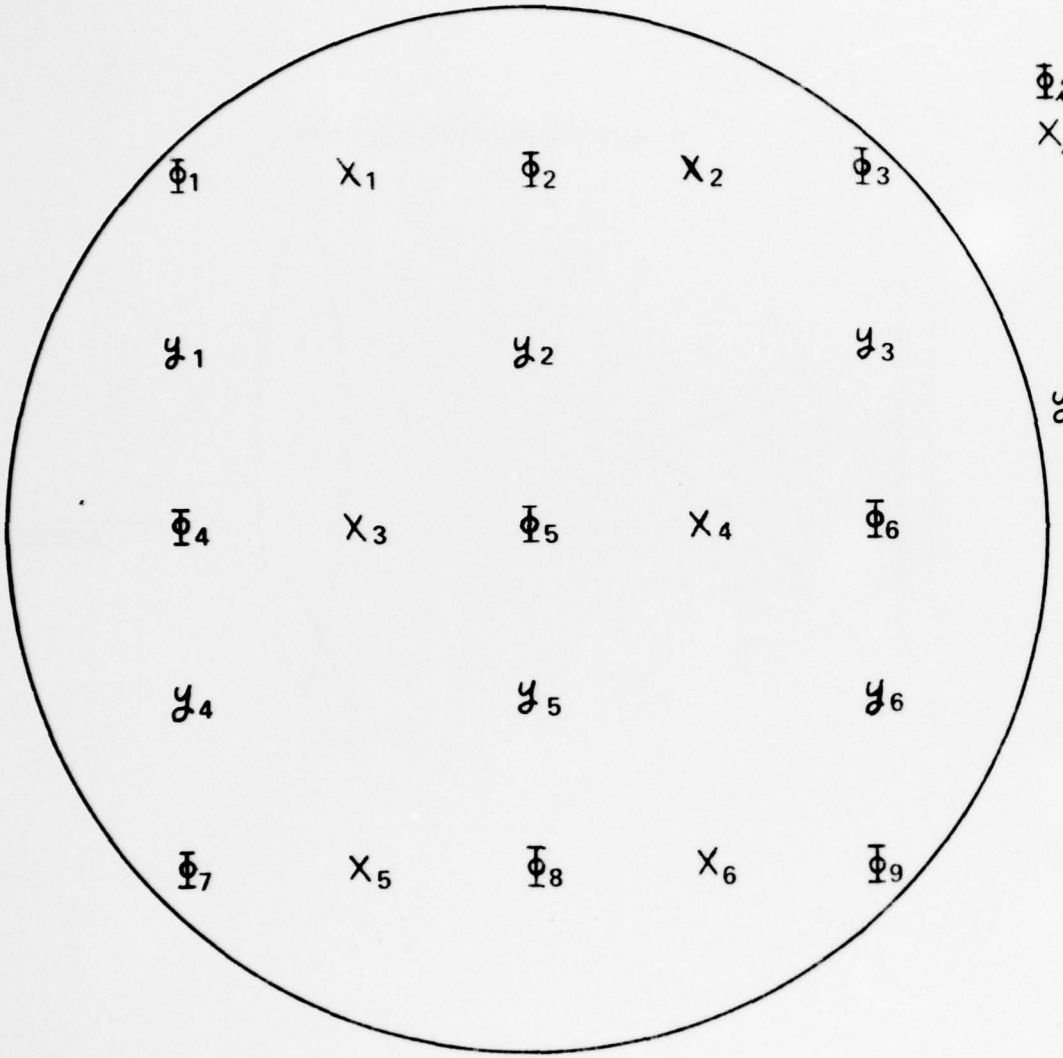

Φ_i = PHASE NATURE

X_i = PHASE DIFFERENCE IN X DIRECTION BETWEEN ADJACENT Φ's (DETECTOR SIGNALS IN X–CHANNEL)

y_i = PHASE DIFFERENCE IN THE Y DIRECTION BETWEEN THE ADJACENT Φ's (DETECTOR SIGNALS IN y CHANNEL)

FIGURE 3 TWO DIMENSIONAL SHEARING INTERFEROMETER

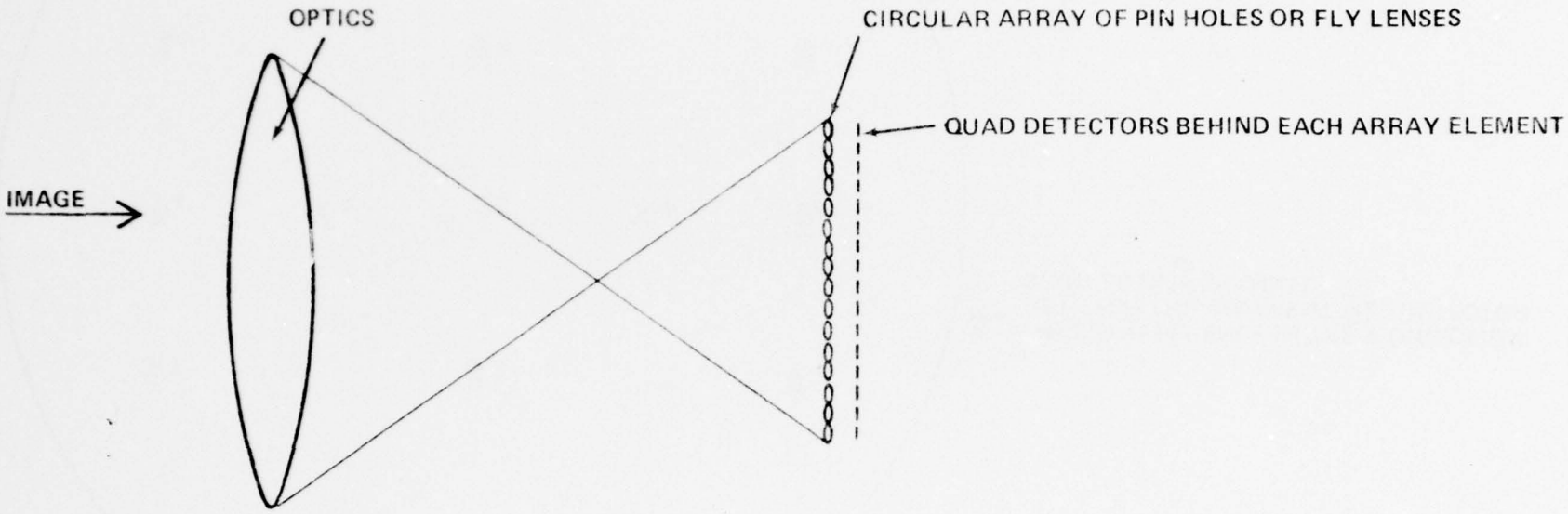

FIGURE 4 HARTMANN ARRAY

References

1. W. B. Bridges, P. T. Brunner, S. P. Lazzara, T. A. Nussmeier, T. R. O'Meara, J. A. Sanguinet, and W. P. Brown, Jr., "Coherent Optical Adaptive Techniques," Applied Optics, Vol. 13, No. 2, pp. 291-300, February 1974.

2. J. E. Pearson, W. B. Bridges, S. Hansen, T. A. Nussmeier, and M. E. Pedinoff, "Coherent Optical Adaptive Techniques: Design and Performance of an 18-Element Visible Multidither COAT System," Applied Optics, Vol. 15, No. 3, pp. 611-621, March 1976.

3. J. E. Pearson, "Atmospheric Turbulence Compensation Using Coherent Optical Adaptive Techniques," Applied Optics, Vol. 15, No. 3, pp. 622-631, March 1976.

4. R. B. Asher and R. Ogrodnik, "Estimation and Control in Multidither Adaptive Optics," to appear in the Journal of the Optical Society of America, March 1977.

5. A. Erteza, "Active Autofocusing Using an Apertured Gaussian Beam," Applied Optics, Vol. 15, No. 9, pp. 2095-2098, September 1976.

6. D. A. Holmes, J. E. Korka and P. V. Avizonis, "Parametric Study of Apertured Focused Gaussian Beams," Applied Optics, Vol. 11, No. 3, pp. 565-574, March 1972.

7. H. J. Robertson, Development of an Active Optics Concept Using a Thin Deformable Mirror, NASA CR-1593.

8. H. J. Robertson, Evaluation of the Thin Deformable Active Optics Mirror Concept, NASA CR-2073.

9. J. F. Creeden and A. G. Lindgren, Control of the Optical Surface of a Thin Deformable Primary Mirror with Application to an Orbiting Astronomical Observatory, Proceedings of the 3rd IFAC Symposium on Automatic Control in Space, 1970.

10. D. MacKinnon, P. Madden, and P. Farrell, Optical Mirror Figure Control, Draper Laboratory Report R-665, May 1970.

11. R. A. Muller and A. Buffington, "Real-Time Correction of Atmospherically Degraded Telescope Images Through Image Sharpening," Journal of the Optical Society of America, Vol. 64, No. 9, pp. 1200-1210, September 1974.

12. J. F. Creeden and H. J. Robertson, "Evaluation of Multipoint Interaction in the Design of a Thin Diffraction Limited Active Mirror," IEEE Transactions on AES, Vol. AES-5, No. 2, pp. 287-293, March 1969.

13. D. Fried, editor, "Special Issue on Adaptive Optics," Journal of the Optical Society of America, March 1977.

14. O. Marcuse, Light Transmission Optics, Van Nostrand Reinhold Co., New York, 1972.

15. V. N. Mahajan, Real-Time Wavefront Correction Through Bragg Diffraction of Light by Sound Waves, Ph.D. dissertation, University of Arizona, 1974.

16. V. N. Mahajan, "Real-Time Wavefront Correction Through Bragg Diffraction of Light by Sound Waves," Journal of the Optical Society of America, Vol. 65, No. 3, pp. 271-278, March 1975.

17. D. Fried, "Statistics of Atmospheric Turbulence," Journal of the Optical Society of America, Vol. 55, pp. 1427-1436, 1965.

18. M. Born and E. Wolf, Principles of Optics, Pergamon Press, New York, Fifth Edition, 1975.

19. J. W. Goodman, Introduction to Fourier Optics, McGraw Hill Book Company, New York, 1968.

20. C. B. Hogge and R. R. Butts, "Frequency Spectra for the Geometric Representation of Wavefront Distortions Due to Atmospheric Turbulence," IEEE Transactions on Antennas and Propagations, Vol. AP-24, No. 2, pp. 144-154, March 1976.

21. R. B. Asher, "Adaptive Estimation of Aberration Coefficients in Adaptive Optics," F.J. Seiler Research Laboratory Report FJSRL TR-76-0017, May 1977, to be submitted to the Journal of the Optical Society of America.

22. R. M. Hawkes and J. B. Moore, "Adaptive Estimation via Sequential Processing," IEEE Transactions on Automatic Control, Vol. AC-20, No. 1, pp. 137-138, February 1975.

23. D. T. Magill, "Optimal Adaptive Estimation of Sampled Stochastic Processes," IEEE Transactions on Automatic Control, Vol. AC-10, pp. 434-439, October 1965.

24. D. G. Lainiotis, "Optimal Adaptive Estimation: Structure and Parameter Adaptation," IEEE Transactions on Automatic Control, Vol. AC-16, No. 2, pp. 160-170, April 1971.